Organometallic Derivatives of Polyphosphazenes as Precursors for Metallic Nanostructured Materials

C. Díaz[1,2] and M. L. Valenzuela[1]

Co-polyphosphazenes containing anchored organometallic fragments are useful precursors for nanostructured metallic materials. Pyrolysis in air at 800°C yields metallic nanoparticles of the type, $M°/M_xO_y/M_z(P_xO_y)/P_4O_7$, depending on the metal used; i.e., M° when the metal is a noble metal, metal oxide when the metal is Cr, W and Ru, metallic pyrophosphate when M = Mn and Fe. The organic spacer of the polyphosphazene influences strongly the morphology of the pyrolytic product. The mechanism of formation of the nanostructured materials involves carbonization of the organic matter, which produces holes where the nanoparticles are grown. Reaction of the phosphorus polymeric chain with O_2 yield phosphorus oxide units, which act as a P_4O_7 matrix to stabilize the nanoparticles and/or $P_xO_y^{-n}$ for the formation of metallic pyrophosphates. The method appears to be a general and versatile new route to metallic nanostructured materials.

KEY WORDS: Metallic nanoparticles; organometallic polymers; polyphosphazenes; pyrolysis.

1. INTRODUCTION

Organometallic compounds as well as polymers are of much interest in materials science [1]. The link between these two types of compounds gives rise to organometallic polymers [2]. These materials exhibit interesting properties specifically because they combine the electronic properties associated with transition metal compounds and the processing advantages of organic polymers. Characteristics routinely associated with transition metals, such as multiple oxidation states and magnetism, are only rarely achieved in organic molecules.

The incorporation of transition metals into a polymer main chain, therefore, clearly offers considerable potential for the preparation of processable materials having properties that differ significantly from those of conventional organic or inorganic polymers. Transition metal-based polymers may also be expected to function as convenient and processable materials for metal-containing ceramics, films, fibers and coatings with high stability and desirable useful physical properties. This review describes the applications of organometallic polymers of the polyphosphazene type with anchored organometallic fragments in nanomaterials science.

Organometallic polymers can be conveniently classified into the following types:

I. Organometallic polymers with transition metals in the main chain.
II. Polymers with organometallic moieties in the side group structure.
III. Polymers with the metal–metal bond in the main chain.

These types of polymers are represented schematically in Scheme 1.

Type I organometallic polymers, containing covalent M-spacer bonds, have been recently reviewed [2a]. On the other hand, type III organometallic polymers,

[1] Departamento de Química, Facultad de Ciencias, Universidad de Chile, Las Palmeras 3425, Santiago, Chile.
[2] To whom correspondence should be addressed. E-mail: cdiaz@uchile.cl

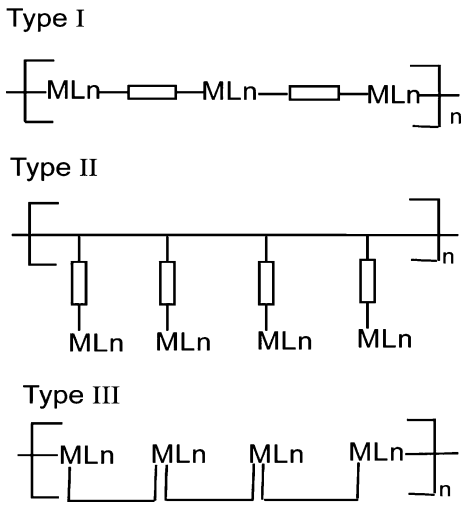

Scheme 1. Classification of organometallic polymers.

having metal–metal bonds, are yet scarce [1d, 2a] and will not be mentioned in this review. Another more general recent review [2c] of organometallic polymers deals mainly with type I polymers and coordination polymers. Type II and III polymers have also been briefly discussed in some select books [1d, e]. The organometallic function in organometallic polymers can arise either from the MLn fragment (which may contain one or more M–C bonds) or from the —[spacer]–C–M linkage. Polymers of the type where ML_n is a coordination fragment is shown in Scheme 2: and the link of the [polymers]-ML_n units does not contain an M–C bond will not be covered in this review. Such types of polymers are often called *coordination polymers*. This topic has been reviewed in a recent article [1c]. Coordination polymers have also been partially mentioned in Refs. [1c, d and 2(c)]. On the other hand, polymers such as *dendrimers* [2a] will not be covered in this review.

From the standpoint of stability and processability, inorganic polymers are most useful in materials science [3]. Among the inorganic polymers, the polyphosphazenes are those that have been most studied due to their advantageous properties and broad applications [1f, 3, 4]. This review attempts to illustrate the use of organometallic derivatives of polyphosphazene in nanomaterials science.

$$[ML_{n-1}\text{-}L'\text{-}ML_{n-1}\text{-}L'\text{-}ML_{n-1}\text{-}L']_n$$

Scheme 2. General formula of coordination organometallic polymer.

Materials with submicron dimensions like nanoparticles represent an exciting new class of substances [5]. As a consequence of their small size, nanomaterials often display unique physical and chemical properties that are atypical of the bulk materials. Optical, magnetic and electrical properties, for instance, are sensitive to size effects. Furthermore, nano-sized particles are also very efficient in the field of catalysis [6] due to their high surface-to-volume ratio. Consequently, numerous processes for nanomaterial synthesis have been investigated with the aim of controlling their size, morphology, structure and chemical composition. A large number of studies on the production of nanoparticles have been published [5]. There exist two main routes to their preparation; e.g., chemical processes using the aqueous method or the sol-gel technique, among others, and physical processes using spray pyrolysis or vapor condensation methods. In this context a solid-phase pyrolytic method is an interesting alternative for preparing nanomaterials, but few experimental methods have been reported. For example, pyrolysis of poly(ferrocenylsilanes) in air yields a red crystalline material of composition SiO_2/Fe_2O_3 [7, 8]. Also, solid-state gold nanoparticles have been obtained by vaporizing a toluene solution to generate Au nanoparticles and pyrolysis of the residue [9, 10]. Another solid-state approach to gold nanoparticles arises from heating solutions of preformed smaller Au particles [11]. Solid-state transition metal nanoparticles included in a SiO_2 matrix have been obtained from a combined sol-gel metal salt inclusion method [12]. And, bimetallic Pt/Pd nanoparticles in the solid state have been obtained by pyrolysis of the organometallic precursor trans-$PtCl(PEt_3)_2SnCl_3$ [13].

A crucial aspect in the formation of nanoparticles both in solution and in the solid state is their stabilization. Stabilization can be electrostatic and steric [14]. Steric stabilization can be achieved through either ligands, polymers, oligomers or solvents. Polyphosphazene polymers $[N = PR_2]_n$ can bind metal ions and organometallic fragments through R-containing donor groups [15–22] (or with the basic nitrogen in some cases). This suggests the possibility of stabilizing metal nanoparticles. In fact, Olshavsky and Allcock [23] reported the preparation in water solution of CdS nanoparticles entrapped in an MEEP (poly(methoxyethoxyethoxy phosphazene)) network. Wisian–Neilson and colleagues [24] prepared gold nanoparticles by reducing $AuCl_4^-$ with $NaBH_4$ in the presence of PMPP (poly(methylphenyl phosphazene)) using a biphasic water/toluene system. Recently,

Wisian–Neilson and colleagues [25] prepared Au nanoparticles using the method of Brust–Schiffrin in water/toluene and stabilizing the nanoparticles with thioether groups anchored to a polyphosphazene backbone. In all these methods the nanoparticles are generated in solution by an independent method, and the polyphosphazene acts as a matrix to stabilize them. Here we review our work on a novel method to produce monometallic and bimetallic nanoparticles from the solid state pyrolysis in air of the organometallic derivatives of the polyphosphazene.

2. SYNTHESIS AND PROPERTIES OF THE ORGANOMETALLIC POLYPHOSPHAZENE PRECURSORS

Two main methods exist for the synthesis of the organometallic derivatives of the copolyphosphazenes: (a) by a substitution reaction of the copolyphosphazene ligand with the respective organometallic compound (Scheme 3), and (b) by reaction of $[(NPR_1R_2)_{1-x}(NPCl_2)_x]_n$ with the respective phenol ligand $HOC_6H_4D{\cdot}ML_n$, in the presence of Cs_2CO_3 and/or K_2CO_3 using acetone as solvent, Scheme 4.

The formulas of some organometallic derivatives of polyphosphazenes prepared by these methods are shown in Table 1.

The organometallic polymers are stable solids whose color depends on the organometallic fragment chromophore: red-brown for 1, 2, 6 and 7; yellow for 3, 4, 8 and 9; green for 5; etc. In general, these materials are insoluble except for 7 and 8. The thermal behavior in nitrogen yields pyrolytic residues in the range of 10–71%, which converts, in some cases, to interesting ceramic materials. The high pyrolytic yield was attributed to the crosslinking of the polyphosphazene chains by the organometallic fragment. Recent IR studies have shown that loss of the carbonyl groups from the transition metal-containing polyphosphazenes by heating produces vacant sites around the metal that induce the coordination of donor groups of the polymeric chain [26]. These results led us to investigate the pyrolytic behavior of the organometallic polyphosphazenes in air.

3. PYROLYSIS OF THE POLYPHOSPHAZENE-CONTAINING ORGANOMETALLIC FRAGMENTS

Pyrolysis in air of the organometallic polymers affords nanostructures whose nature depends on the metal, the organic spacer of the polymer, and the charge of the copolymer unit containing the organometallic fragment (see Scheme 5).

Results depend on the metal involved or the nature of the nanostructured metallic materials. In this review we will discuss the first option.

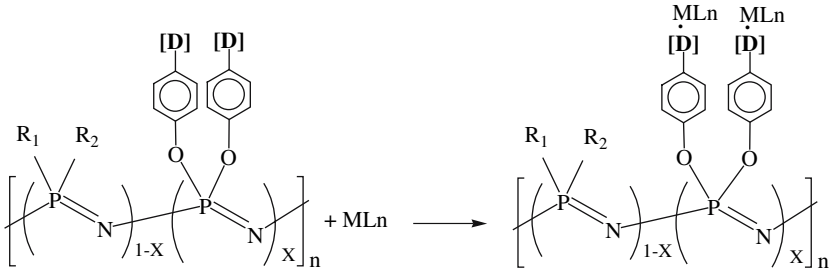

Scheme 3. Reaction showing the general formation of organometallic polymer from a polymer ligand and a organometallic fragment.

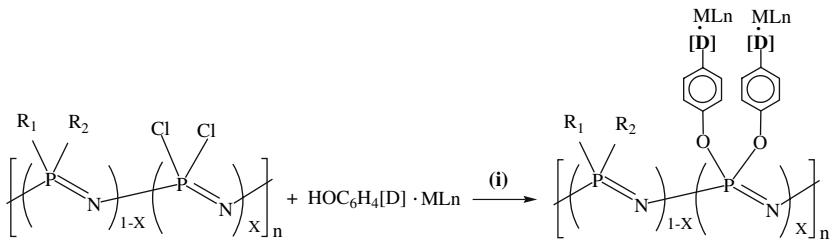

Scheme 4. Reaction showing the general formation of organometallic polymer from the $[PCl_2]_n$ and the P-functionalized donor phenol. (i) Denotes the reaction conditions: K_2CO_3 and acetone as solvent.

Table 1. Formulas for the type II organometallic derivates of polyphosphazene

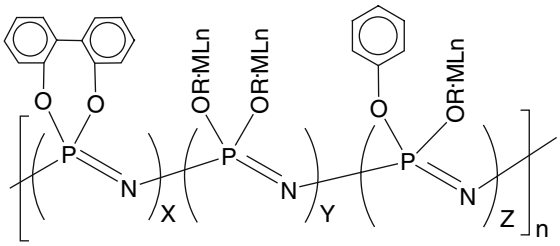

Polymer	R	ML_n	*X*	*Y*	*Z*	Ref.
1	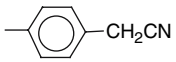	$C_pFe(dppe)$	0.80	0.18	0.02	[21]
2	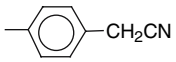	$C_pFe(dppe)$	0.55	0.20	0.25	[21]
3	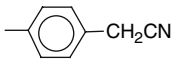	$C_pRu(PPh_3)_2$	0.80	0.18	0.02	[21]
4	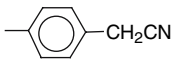	$C_pRu(PPh_3)_2$	0.55	0.20	0.25	[21]
5	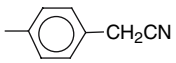	$Cr(CO)_5$	0.80	0.18	0.02	[16]
6	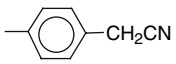	$(\pi–CH_3–C_5H_4)Mn(CO)_2$	0.55	0.20	0.25	[18]
7	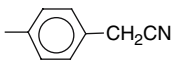	$C_5(CH_3)_5Fe(dppe)$	0.80	0.18	0.02	[20]
8	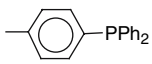	$(\pi–CH_3–C_5H_4)Mn(CO)_2$	0.60	0.40	0.0	[29]
9		$W(CO)_5$	0.65	0.35	0.0	[22]

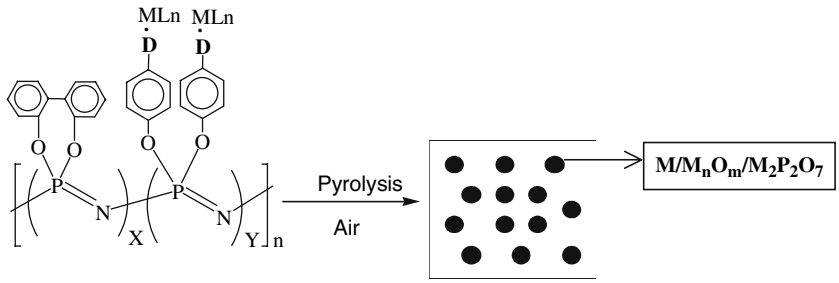

Scheme 5. Schematic representation of the solid-state pyrolysis of the organometallic polyphosphazene.

3.1. Polyphosphazene Containing the $Cr(CO)_5$ Fragment

Pyrolysis of the organometallic polymer of approximate composition $\{[\{NP(O_2C_{12}H_8)_2\}_{0.8}\{NP(OC_6H_4CH_2CN)_2\}_{0.18}][Cr(CO)_5\}_{0.132}]_n$ in air yields a light-green solid in a pyrolytic yield of 11% [27]. The material was characterized by IR, XRD, SEM-EDAX and TEM. The transmission electron

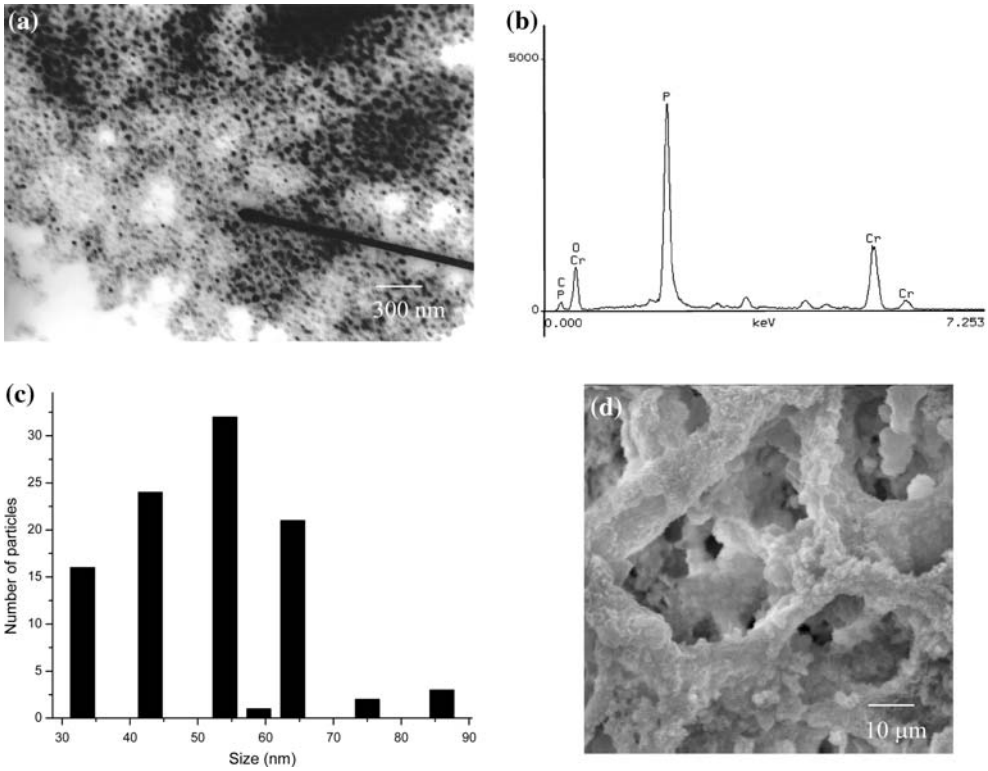

Fig. 1. Experimental data of the pyrolysis of the organometallic polyphosphazene (5). (a) TEM, (b) EDAX, (c) size histogram, and (d) SEM.

microscopy image, Fig. 1(a), shows clearly the formation of nanoparticles.

The presence of chromium is evident from the EDAX shown in Fig. 1(b) . The histogram shows a mean particle size of 54 nm. Finally, IR, Raman and X-ray diffraction analyses are consistent with the presence of nanoparticles of Cr_2O_3 inside a P_4O_7 matrix. Thermal analysis of the organometallic polymer also supports this composition. The pyrolysis experiments showed that the product was etched on the ceramic crucibles, opening a potential way for imprinting metal oxides on ceramic surfaces with possible applications in advanced ceramic technologies.

3.2. Polyphosphazene Containing the $W(CO)_5$ Fragment

Organometallic polymers of the type $\{[NP(O_2C_{12}H_8)]_x\ [NP(OC_5H_4N{\cdot}W(CO)_5)]_y\}_n$, $x = 0.7$, $y = 0.3$; $x = 0.8$, $y = 0.2$ were pyrolyzed in air to give white materials formulated as W/WO_3 mixtures [28]. However, the pyrolytic residues were not totally homogenous and zones rich in WP_2O_3 were also detected. Figure 2 shows the SEM image and the EDAX analysis of the pyrolysis product, $\{[NP(O_2C_{12}H_8)]_{07}\ [NP(OC_5H_4N{\cdot}\ W(CO)_5)]_{0.3}\}_n$, (a) and (b), and for $\{[NP(O_2C_{12}H_8)]_{0.8}\ [NP(OC_5H_4N{\cdot}\ W(CO)_5)]_{0.2}\}_n$. (c) and (d). A similar "Gruyère-cheese" morphology was observed for both products. The presence of mainly W in their EDAX was consistent with the formulation of the products.

A plausible mechanism of formation of the W materials was suggested on the basis of the thermal study in air. The first step was the loss of the carbonyl groups from the tungsten atoms. Following this, calcination of the organic matter produced holes in the polymeric matrix, causing the agglomeration of the metallic centers. In the latter step some WO_3 was also obtained by oxidation of the previously formed W^o. Subsequently, oxidation of the nitrogen and phosphorus of the polymeric chains formed nitrogen oxides, which are volatile at these temperatures and are lost, and phosphorus oxides, which behave both as matrix stabilizers and as sources of phosphates to form some tungsten phosphates. In view of the interest in applications of WO_3, the preparation method given here can be a reliable route to both W and WO_3.

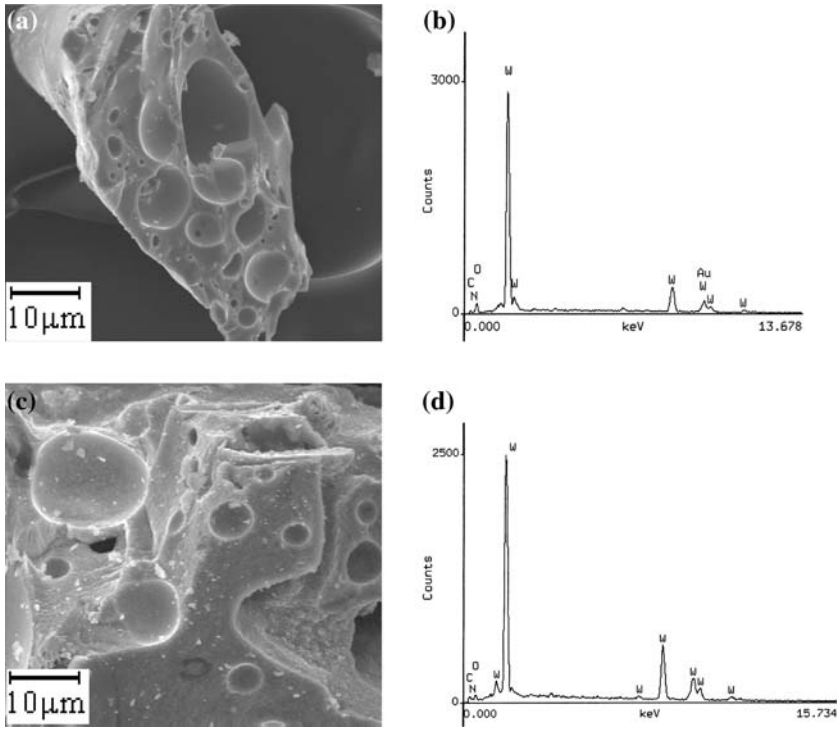

Fig. 2. SEM micrograph and EDAX analysis of pyrolysis residues from $\{[NP(O_2C_{12}H_8)]_{0.7}\ [NP(OC_5H_4N{\cdot}\ W(CO)_5)]_{0.3}\}_n$ [(a) and (b)] and $\{[NP(O_2C_{12}H_8)]_{0.8}\ [NP(OC_5H_4N{\cdot}\ W(CO)_5)]_{0.2}\}_n$ [(c) and (d)].

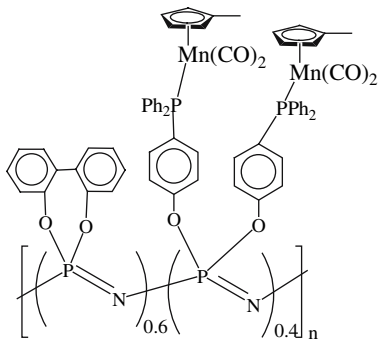

Scheme 6. Formula of the organometallic derivative of the polyphosphazene with the anchored Mn-fragment.

3.3. Manganese Cymantrene Fragments Anchored to Polyphosphazene

Pyrolysis of the copolyphosphazenes, containing the anchored organometallic fragment $CH_3C_5H_4Mn(CO)_2$ and the approximate formula [29] in Scheme 6, affords a light-pink solid in a 26–29% yield [30]. TEM analysis of the materials shows clearly the formation of nanostructures (Fig. 3(a)).

An X-ray diffraction analysis is consistent with the presence of monoclinic $Mn_2P_2O_7$. The histogram indicates a mean particle size of 74 nm and the EDAX analysis shows the presence of manganese, phosphorus and oxygen. The material exhibits near-infrared photoluminescence attributed to the emission of isolated tetrahedral Mn^{2+} embedded in a MnP_2O_7 matrix. Figure 4 shows the solid-state photoluminescence spectrum of the product.

3.4. Copolyphosphazene Containing the $CpRu(PPh_3)_2^+$ fragment

Pyrolysis of the yellow organometallic polymer (Scheme7) in air yields 14–7% of a black-green solid identified as mainly RuO_2 [31]. The morphology of the product formed upon thermolysis of the Ru organometallic polymer, determined by SEM, is shown in Fig. 5(a).

The morphology of the pyrolytic material shows a dense ceramic-like structure [32] with some pores. Typical fractures of mortar-like materials are also seen.

Elemental analysis of the material by EDAX (Fig. 5(b)) in several zones (indicated by the arrows in Fig. 5(a)) of the material indicates a uniform

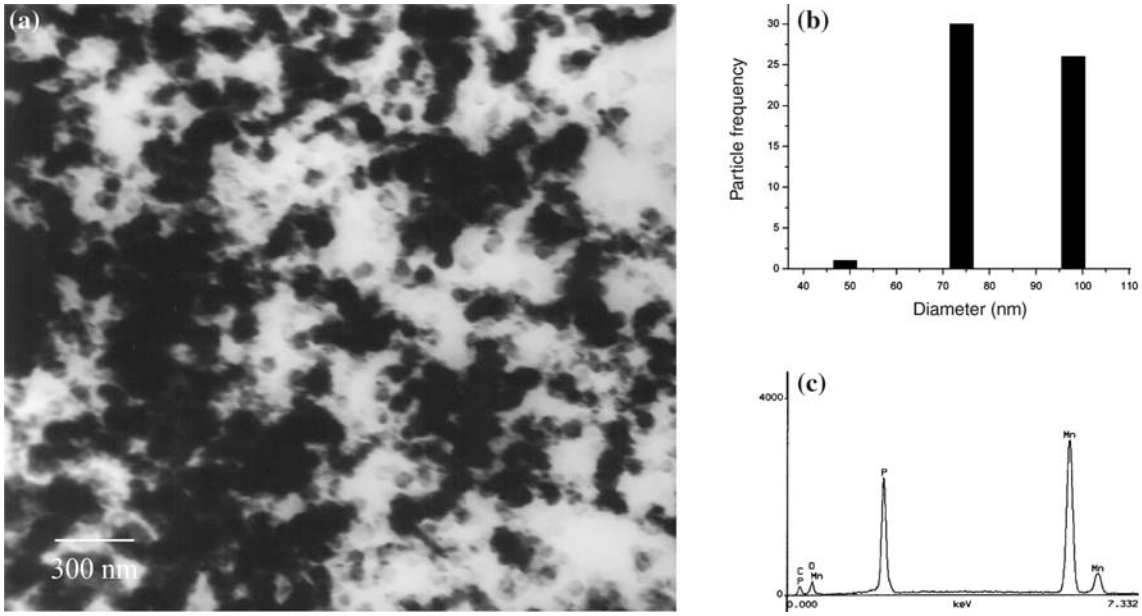

Fig. 3. TEM (a), histogram (b) and EDAX (c) of the pyrolysis product from the polymer $\{[NP(O_2C_{12}H_8)]_{0.6}[NP(OC_6H_4PPh_2 \cdot (\pi\text{–}CH_3C_5H_4)Mn(CO)_2)_2)]_{0.4}\}_n$.

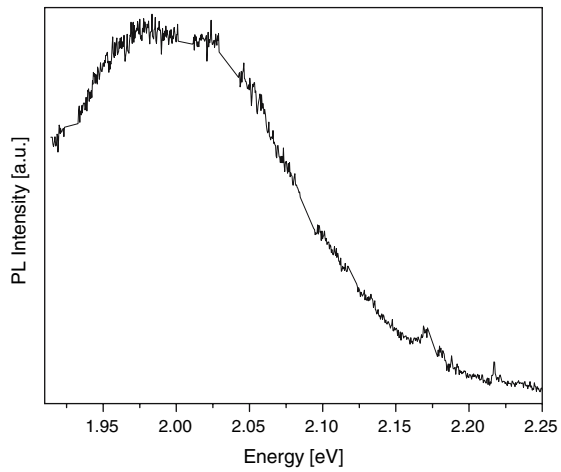

Fig. 4. Solid-state photoluminescence spectrum of pyrolysis product.

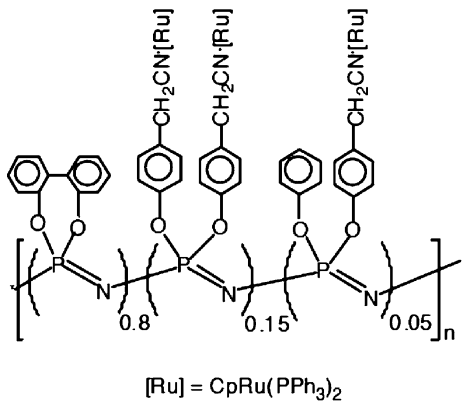

Scheme 7. Approximate representation of the structure of Ru organometallic polyphosphazene polymer.

composition. Values close to RuO_2 are seen, with the one measured in zone 2 closest to that calculated for RuO_2. TEM images of the material, shown in Fig. 5(c), show nanostructures with several shapes, some of them circular. Estimation of the diameter of some of the most regular circles gave values close to 10 nm.

As found for tetragonal RuO_2, the pyrolysis product displays an antiferromagnetic interaction. Magnetic susceptibility measurements were made in the 5–300 K range. Figure 5(c) shows the μ_{eff} and χ_m versus temperature profile, which is indicative of an antiferromagnetic interaction. However, the ambient temperature magnetic moment, $\mu = 1.69$ BM, is somewhat higher than the corresponding value for pure RuO_2, $\mu = 0.78$ BM [33]. The lower value reported for pure RuO_2 has been attributed to the rutile structure, which permits an antiferromagnetic interaction [33].

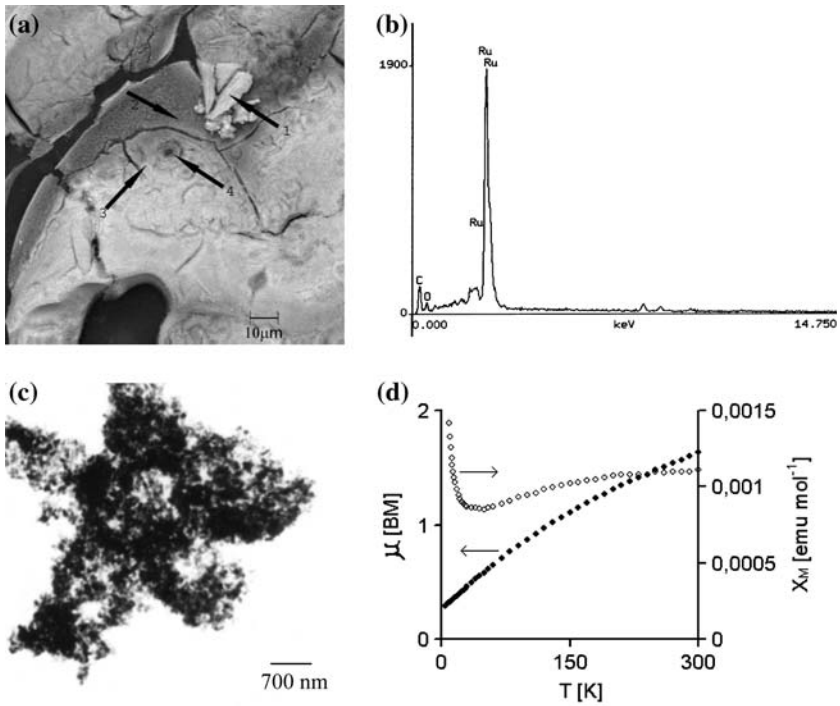

Fig. 5. SEM (a), EDAX (b), TEM (c) and variable temperature susceptibility (SQUID) (d) of the RuO_2 product from pyrolysis.

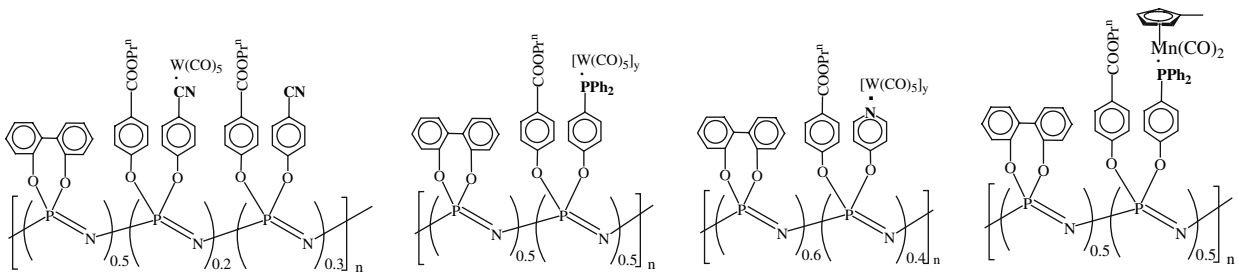

10 **11** (y = 0.7) y = 1 (**12**); y = 0.4 (**13**) **14**

Scheme 8. Approximate formulas for the organometallic polyphosphazene with $W(CO)_5$ and CH_3–C_5H_4–$Mn(CO)_2$.

4. INFLUENCE OF THE NATURE OF THE DONOR SPACER AND METAL, ANCHORED TO THE POLYMER CHAIN, ON THE MORPHOLOGY OF THE NANOSTRUCTURED MATERIALS

The series of organometallic polyphosphazenes shown in Scheme 8 offers the opportunity to compare the different morphologies of the pyrolytic residues as a function of the nature of both the donor links to the spacer; i.e., OC_5H_4N and $OC_6H_5PPh_2$, and W compared to Mn [26, 34]. With the same metal, tungsten for instance, the polymer containing the diphenylphosphine spacer and, as observed for other polymer containing the same spacer [28], a mostly Gruyère-cheese-type morphology was found, in contrast to the similar polymer containing the pyridine spacer, where a mostly dense morphology was found for the pyrolytic residue. Figure 6 illustrates this point. On the other hand, with the same spacer, the diphenylphosphine for example, manganese shows a more porous pyrolytic material than that containing with tungsten, as shown in Figs. 6(a) and (c).

On the other hand, the nature of the pyrolytic residues is similar to those containing spacers $OC_6H_4PPh_2{\cdot}CH_3$–$C_5H_4Mn(CO)_2$. and $OC_6H_4PPh_2{\cdot}W(CO)_5$, namely mainly $Mn_2P_2O_7$ [30] and a previously described mixture of W and WO_3 [28].

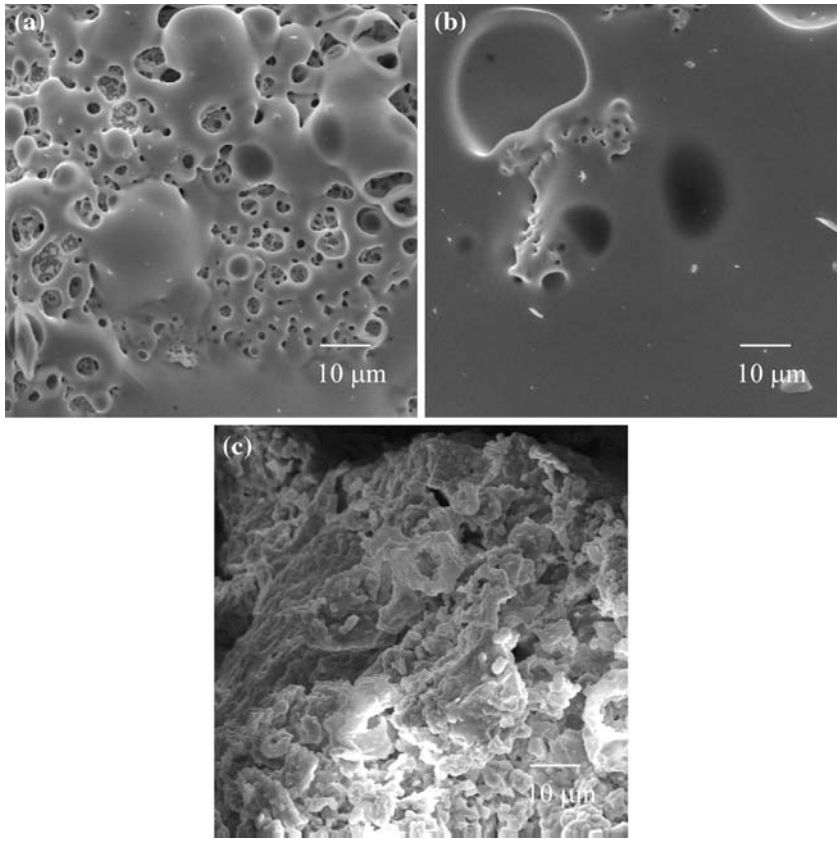

Fig. 6. SEM image of pyrolytic products from 11(a), 12(b) and 14(c).

5. COPOLYPHOSPHAZENE CONTAINING THE CPFE(DPPE)$^+$ FRAGMENT: MONO AND BIMETALLIC NANOPARTICLES

The iron-containing polyphosphazene copolymers 15–17 were prepared as reported previously (Scheme 9) [21]:

In the formula of products **15**, Fe represents the organometallic CpFe(dppe)$^+$ fragment; the respective counter ion, PF_6^-, is not in the scheme. In polymer **17**, $TlPF_6$ is linked to the chain in a unknown manner. Pyrolysis of the copolymers in air gives white solids **15′** and **17′** in yields from 27 to 30% [35]. Figure 7(a) shows the TEM micrograph of the pyrolytic product **15′**.

Some irregular shapes were seen. Where the particles are nearly circular, a mean size of 56 nm was estimated (Fig. 7(b)). The XRD scan of **15′** showed the expected signals for $Fe_2Fe_5(P_2O_7)_4$ (Fig. 7(c)). Similar XRD signals were found for pyrolytic product **16′**. The positions and relative intensities of the XRD peaks match well the known XRD pattern of $Fe_2Fe_5(P_2O_7)_4$ (see arrows). For both **15′** and **16′**, other less intense peaks in the zone $2\theta = 14°–20°$ (see circles) are attributed to phosphorus oxides, which act as a stabilizing matrix for the $Fe_2Fe_5(P_2O_7)$. Surprisingly, when the reaction (Scheme 9) was performed in presence of $TlPF_6$ (product **17′**) and pyrolyzed, bimetallic structures were obtained. Figure 8(a) shows the EDAX analysis, where the presence of iron and thallium is clearly seen. However, the morphology was similar to that of products **15′** and **16′** as shown in Fig. 8(b).

The TEM image of the bimetallic materials shows the Tl nanoparticles as the darker dots and the surrounding iron shells (Fig. 8(c)). From some of the most regular circles, the histogram based on the Fe/Tl nanoparticles in Fig. 8(c) shows a means particle size of 50 nm, with the core having a mean size of 20 nm. Thus, the TEM is typical of core-shell nanoparticles [36–38]. In Fig. 8(c), the nanoparticles, which have the higher Z (atomic weight) compared to the Fe particles appear as the darkest dots. We propose a core-shell shape for the bimetallic nanoparticles, with the $Tl_3P_3O_9$ nanoparticles forming the core and

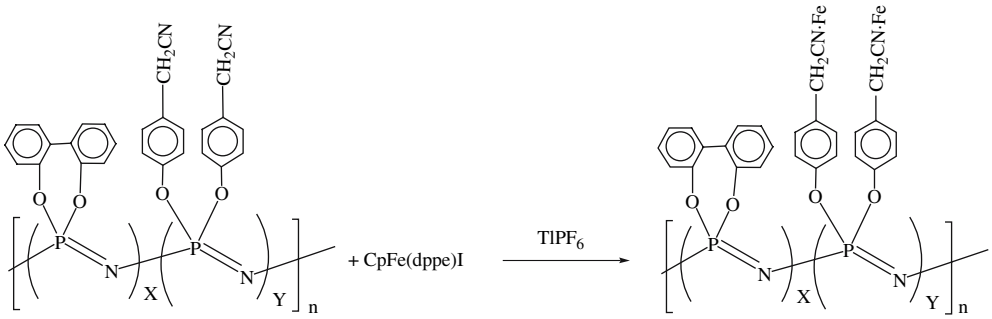

X	Y	Nº	Pyrolytic Product
0.8	0.15	(15)	(15)'
0.55	0.25	(16)	(16)'
0.8	0.15	(17) with $TlPF_6$	(17)' with $TlPF_6$

Scheme 9. Reaction scheme for the formulation of the polyphosphazene having an Fe fragment anchored.

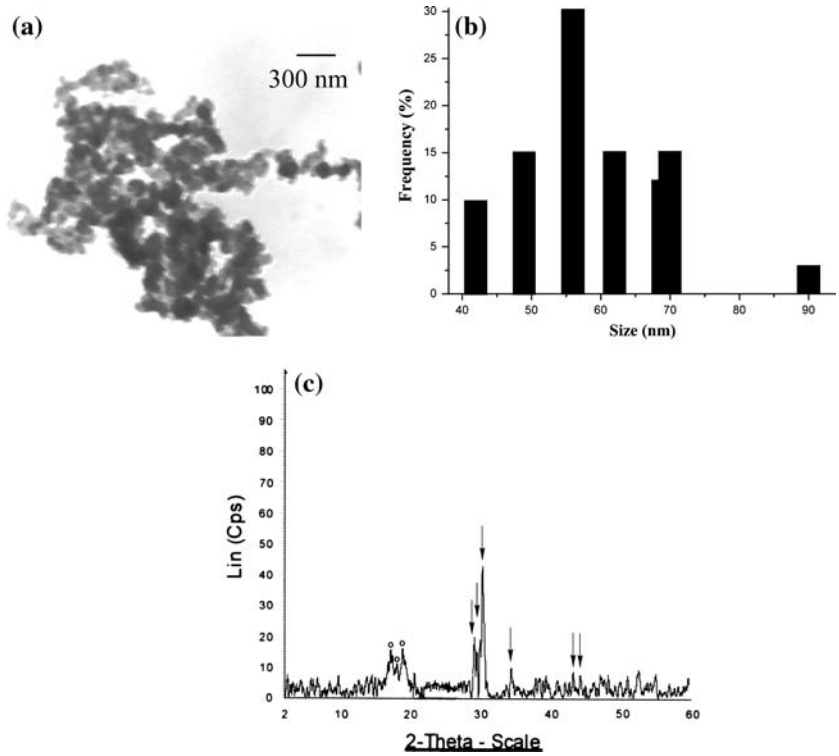

Fig. 7. TEM micrograph of pyrolytic product **15′** (a), the size histogram (b) and the XRD pattern (c).

$Fe_2Fe_5(P_2O_7)_4$ the shells. As for product **15′**, the composition of the nanoparticles was determined by XRD analysis.

The more abundant phosphorus oxides compared to the Tl and Fe metals (due to the partial coordination of the organometallic fragment to the polymer [21]) induce P_4O_7 to act as stabilizing as is shown in model depicted in Fig. 9. Similarly, the lower content of Tl than Fe leads to a core/shell nanoparticle as shown in Fig. 9. This mechanism was proposed, among others, considering the thermal studies of the iron polymers.

From these results we conclude that incorporation of two organometallic fragments in the polyphosphazenic chain and its subsequent pyrolysis in air could yield bimetallic nanostructured materials. The procedure could be a general method for the synthesis of varied bimetallic nanostructured materials. Experiments to corroborate this are under way.

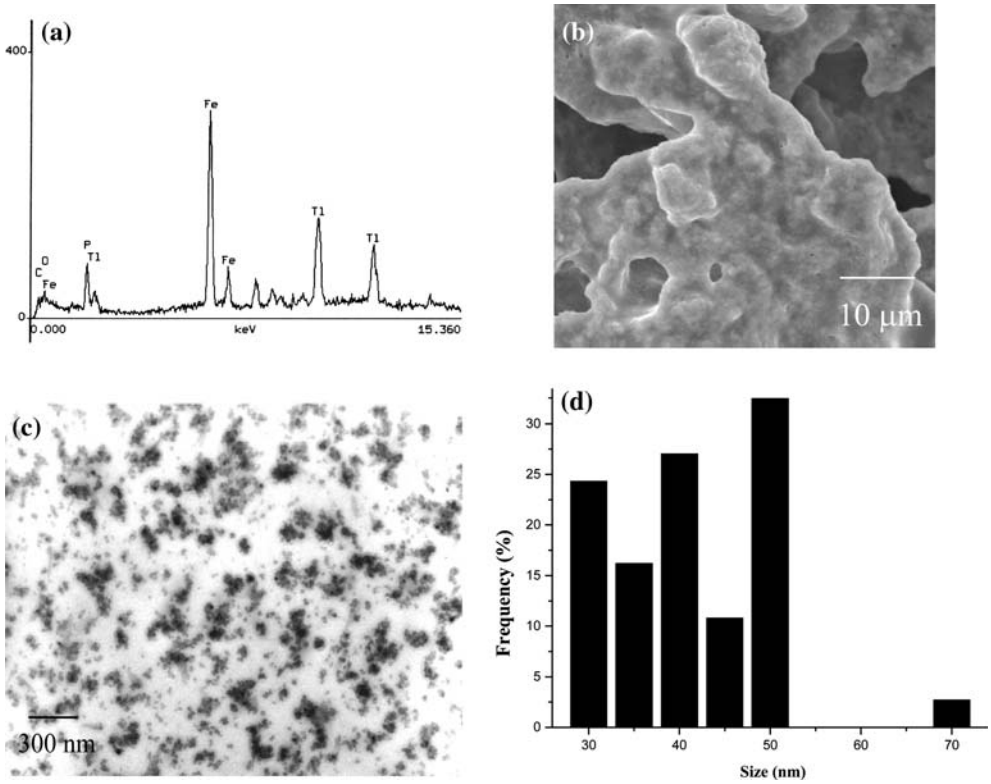

Fig. 8. EDAX (a), SEM (b), TEM (c) and size histrogram (d) of the bimetallic nanostructured material **17′**.

6. COPOLYPHOSPHAZENE CONTAINING NOBLE METAL ORGANOMETALLIC FRAGMENTS

Incorporation of gold in the polyphosphazene chain containing pyridine as a donor and using the organometallic fragment $Au(C_6F_5)$ gave the polymer shown in Fig. 10 [39].

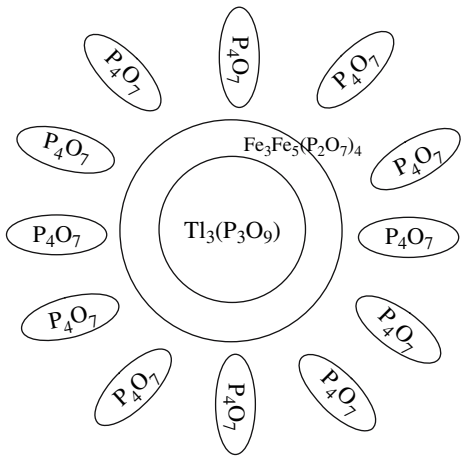

Fig. 9. Proposed model of the nanoparticles formed from pyrolysis of 7.

Pyrolysis of the Au organometallic polymer at 800°C in air yields a reddish-yellow solid in a 29% yield. The nanostructured Au materials obtained have a monolithic morphology as shown in the SEM images in Figs. 11(a) and (b).

The EDAX analysis confirms the presence of only Au as seen in Fig. 11(c). The RDX patterns show characteristic peaks corresponding to cubic Au (Fig. 11d). The nanostructured Au can be etched on the ceramic crucible surface, a quartz surface and a silicon wafer surface without suffering the loss of the Au with acids, bases or physical

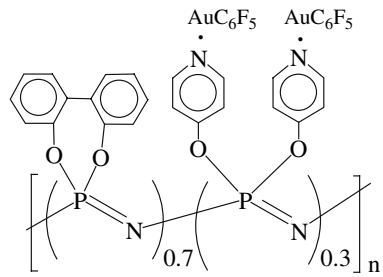

Fig. 10. Formula of polymer **18**.

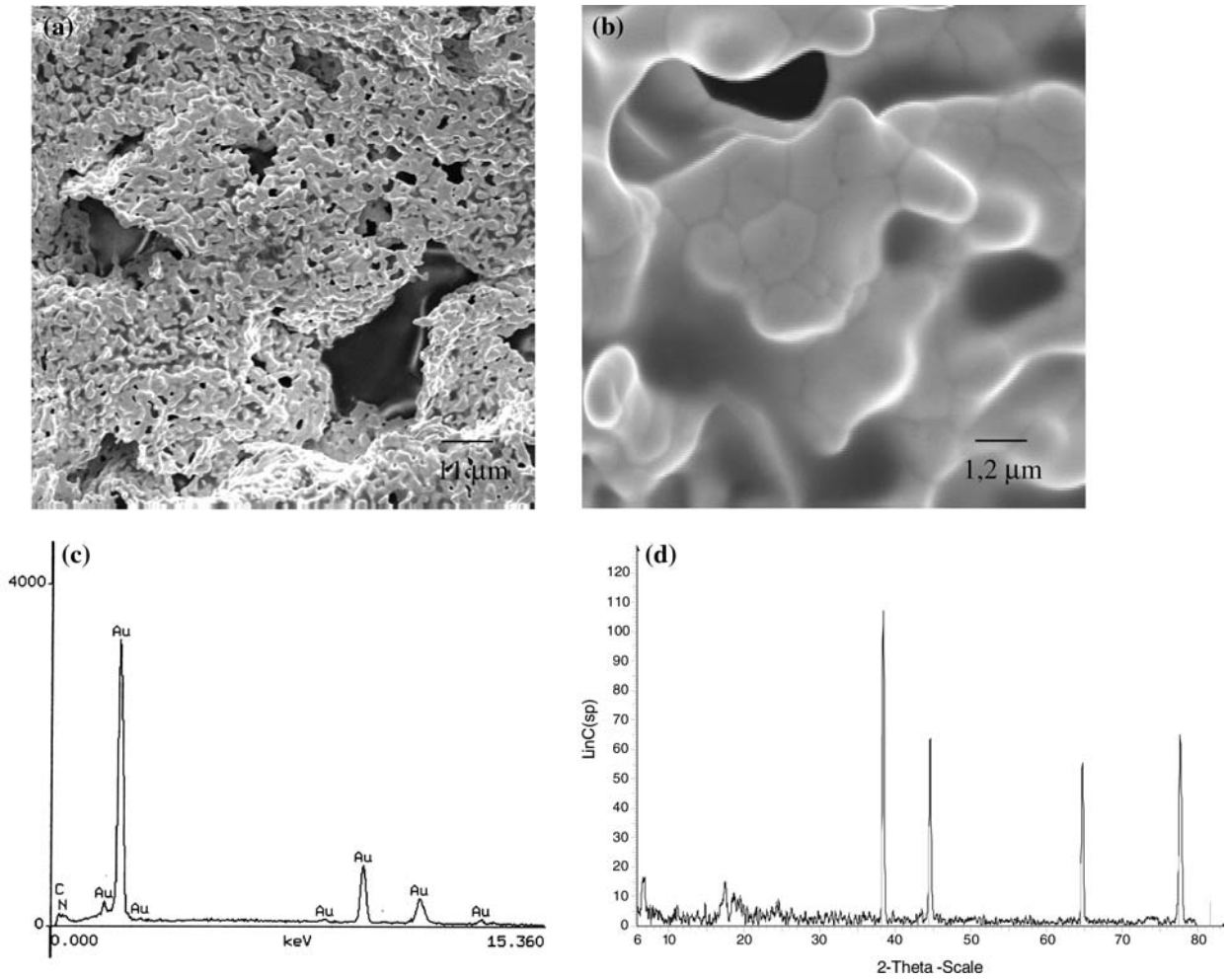

Fig. 11. SEM (a), (b) at different magnifications, EDAX (c) and RDX (d) for pyrolytic residue **10**.

methods. Figure 12(a) shows a line drawing made by etching a sample of the polymer on the surface of a ceramic crucible.

Figure 12(b) shows an SEM image of Au etched on the crucible, which is indicated by the arrow marked (1), and the zone of the ceramic crucible, which is indicated by the arrow marked (2). EDAX that is focused on zone (1) and marked by the point of the arrow shows clearly the presence of Au as well as the ceramic elements, Si, Al, K, Ca and Na (Fig. 12(c)). In Fig. 12d, the EDAX analysis in the zone that is marked by the point of arrow (2) shows clearly *only* the presence of the ceramic materials.

7. MECHANISM OF FORMATION OF NANOPARTICLES

Thermogravimetric (TG) studies in air indicate a common and general mechanism of formation of nanoparticles from pyrolysis of the organometallic polymer. In almost all of the TG studies, the first step involves carbonization of the organic matter and a small weight loss was also seen and attributed to the decomposition of the organometallic fragment. This step produces a mixture of CO/CO_2 that forming holes, which allow the agglomeration of the metallic nanoparticles. The formation of the metal oxide nanoparticles can occur in two ways: (i) Oxidation of

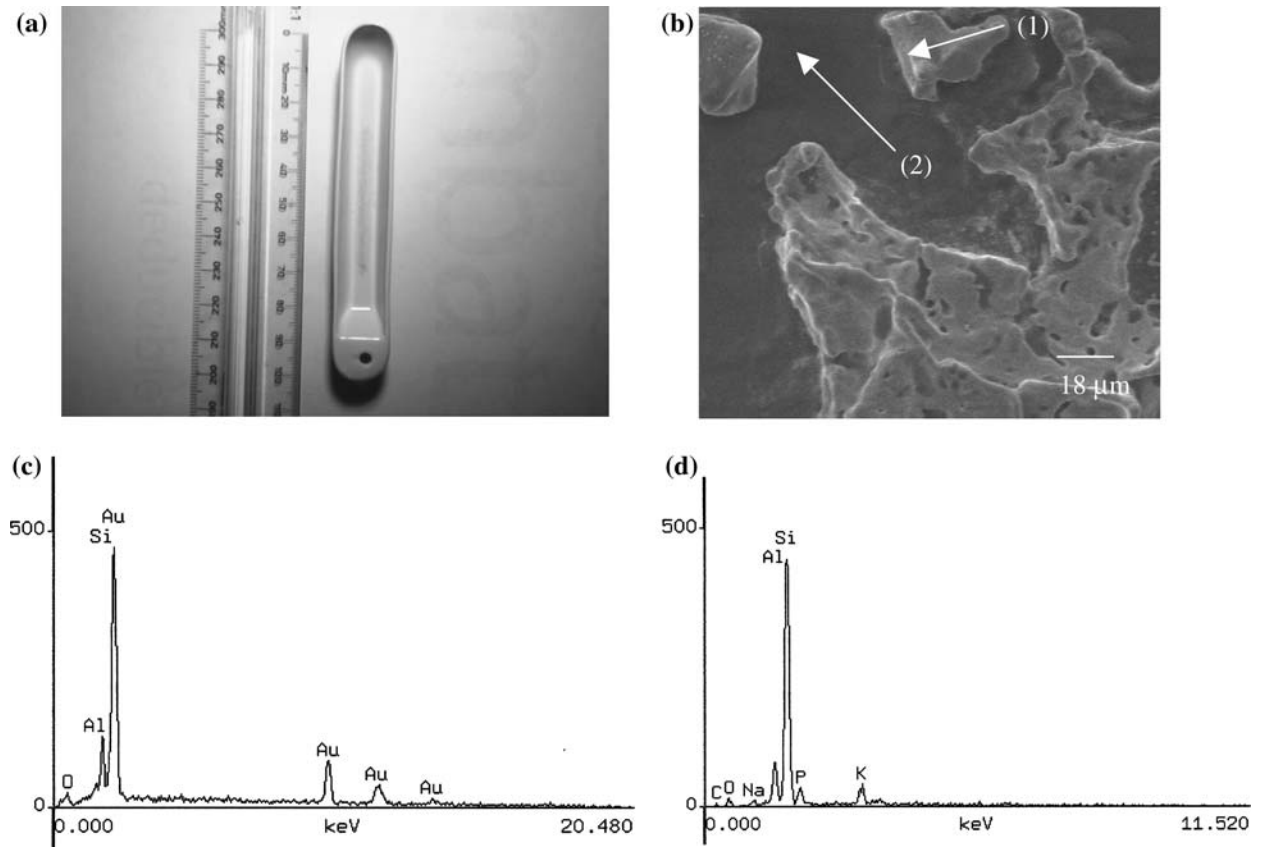

Fig. 12. Thermo-etching on a boat crucible of polymer **18**. (a) SEM of the deposited Au film; (b) arrows indicate two zones where EDAX was performed: EDAX (c) zone 1 and EDAX (d) zone 2.

the previously formed metal in oxidation state zero (formed by reduction with CO/CO_2 mixtures of the corresponding M^{n+} ion [12]) or (ii) reaction of the M^{n+} ion, for instance polymer 6, with O_2. The metal pyrophosphate-nanostructured salts can be formed by simple reaction of the Mn^{n+} ions (similarly with Fe) with the pyrophosphate anions formed *in situ* from oxidation of the phosphazene P atoms; e.g., $Mn^{2+} + P_2O_7^{=} \longrightarrow Mn(P_2O_7)$. In all the cases, the low metal/P, N ratio produces excess P_4O_7 units, which act as a stabilizing matrix for the nanoparticles. Figure 13 shows a general and representative TG curve of an organometallic derivative containing polyphosphazene. In agreement with the proposed mechanism, the pyrolysis of a carborane polyphosphazene derivative (Scheme 10) yields nanostructured BPO_4 [40], which usually is formed by reaction of B_2O_3 with P_2O_5 [41].

A cartoon representation of the general mechanism of the formation of metallic nanoparticles is given in Fig. 14.

8. PYROLYSIS OF POLYPHOSPHAZENE CONTAINING SILICON FRAGMENTS

Allcock has reported the first family of polyphosphazene containing silicon fragments anchored to the polymeric chain [42–46]. Polymers of this type are shown in Scheme 11 and were prepared from the partial lithiation reaction of the $\{[NP(OCH_2CF_3)]_x[NP(Cl)_2)]_y\}_n$ intermediates followed by coupling of the chlorosilanes [44], by ring-opening addition of the respective phosphazene trimer [43], or by reaction of the intermediate with the respective amines in the presence of triethylamine [45–46]. Also polyphosphazenes containing silicon anchored groups of the type $\{[NP(OC_6H_4Br)(OC_6H_4R)]_x[NP((OC_6H_5)(OC_6H_4R)]_y\}_n$ with $R = SiMe_3$, $SiMe_2Ph$ and $SiMePh_2$ were also prepared by Allcock by known metal–halogen exchange reaction of poly[bis(*p*-bromo-*p*-phenoxy)phosphazene] with *n*-BuLi at −78°C [44]. However, as Allcock and Coggio noted [45], the synthesis of this type of polymer containing

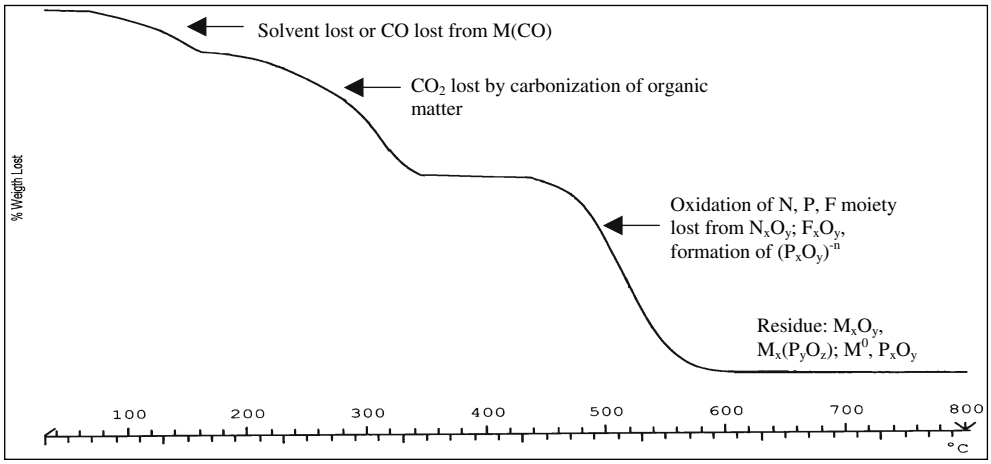

Fig. 13. Representative TG of an organometallic polyphosphazene.

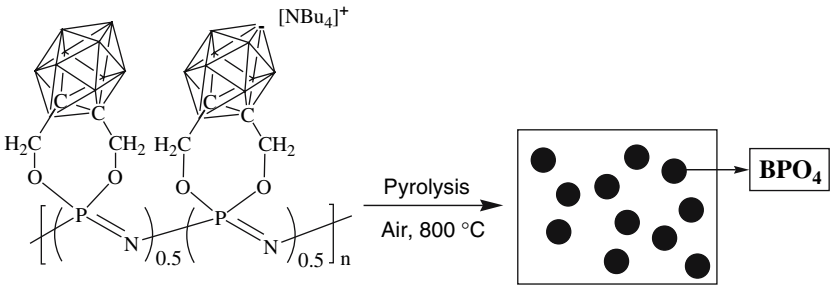

Scheme 10. Schematic representation of the formulation of nanostructured BPO_4 from pyrolysis of **19**.

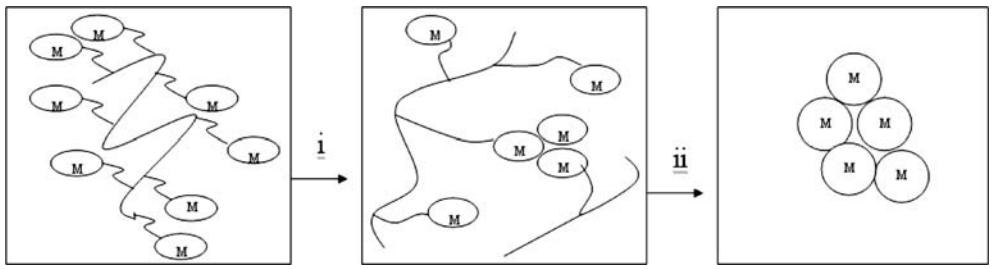

Fig. 14. Proposed mechanism for the formation of metallic nanoparticles from the pyrolysis of polymer; (i) Metal release from the polymer and partial calcination of the organic matter. (ii) Nucleation and growth of the metal-nanostructured material (here M represents the metallic nanoparticle: i.e., oxide, phosphate or metal. The matrix formed by P_4O_7 that surrounds the metallic compound is not indicated.

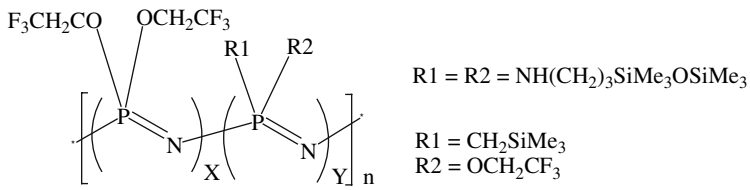

Scheme 11. Formula of silylated polyphosphazene prepared by Allcock.

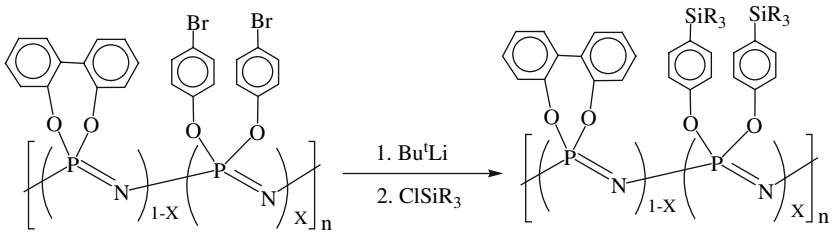

Scheme 12. Schematic formation of silyl-containing polyphosphazene (20) from the bromide intermediate polymer; R = CH_3.

anchored silicon groups is, in general, quite difficult. Most recently Allcock has reviewed the chemistry of phosphazene-organosilicon oligomers [47] and polymers [48].

In a similar way we have recently prepared the polyphosphazene containing a silicon fragment anchored to the polymeric chain as shown in Scheme 12 [49]:

Pyrolysis of these polyphosphazenes containing silicon fragments was studied in air at 600, 800 and 1000°C. The morphology and composition of the pyrolytic products depend on the temperature of the pyrolysis, as shown in Fig. 15. The products can be formulated as a complex mixture that contains SiP_2O_7 and SiO_2.

9. CONCLUSIONS

In this account we have summarized briefly our earlier work as well as our recent results on the synthesis and characterization of polyphosphazenes containing anchored organometallic fragments and their conversion into nanostructured metallic materials.

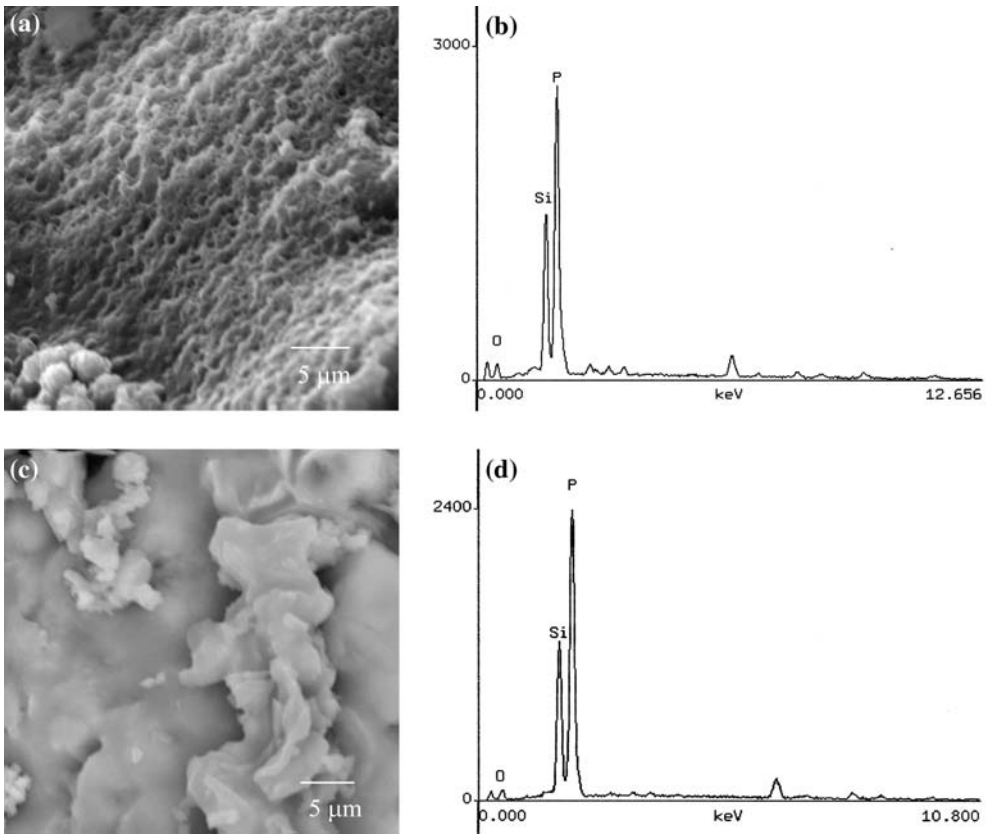

Fig. 15. SEM and EDAX image of the pyrolysis products at several temperatures. (a) and (b) at 600°C; (c) and (d) at 800°C.

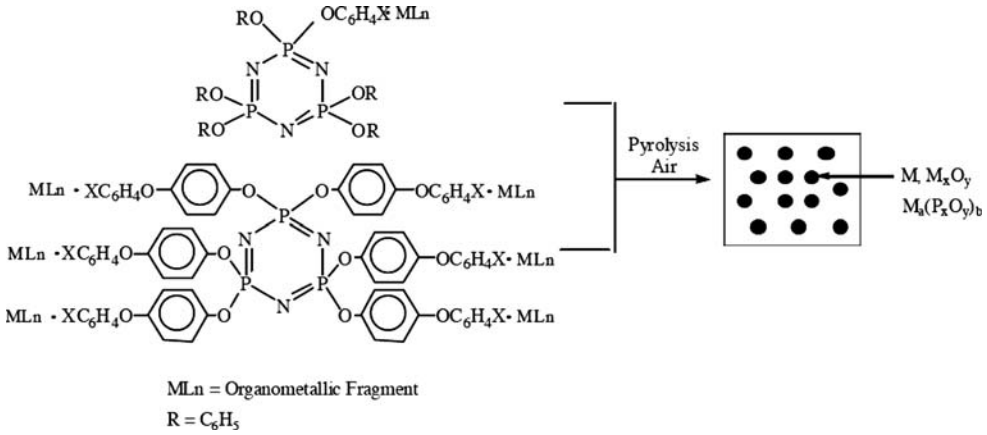

Fig. 16. Schematic representation of the solid-state pyrolysis of the organometallic phosphazene trimer.

The materials from the pyrolysis of the phosphazene polymers depend on the nature of the metal, the nature of the spacer polymer, the charge on the organometallic fragments, and the pyrolysis temperature. With organometallic fragments containing transition metals, such as Cr, Ru and W, the metal oxide is obtained. On the other hand, with metal like Mn and Fe. metallic pyrophosphates are obtained. As could be anticipated, with noble metals like gold, the metal is obtained. The nature of the polymer spacer strongly influences the morphology of the pyrolytic product. The phosphorus atom of the polymeric chain after burning forms phosphorus oxides, which are stable at the pyrolysis temperature and act both as anions for the nanostructured salts (e.g., pyrophosphates) and/or as stabilizers of the nanoparticles in the solid state (e.g., P_4O_7).

The solid-state pyrolysis of organophosphazene/organometallic (SSPO) methodology described in this review has the following main advantages:

- Versatility: By selecting the appropriate organometallic fragments we can prepare metal nanoparticles with predetermined properties.
- Stability: The solid state of the product allows its incorporation in a solid matrix.
- High metal concentration.

On the other hand, the main disadvantages are:

- Low yields.
- Long and tedious synthetic procedures.
- Broad size distributions (this aspect, however, is common in solid state methods for obtaining nanoparticles).

10. FUTURE POSSIBILITIES

Some of the main disadvantages of the method may be resolved by using organometallic derivatives of the cyclophosphazene trimer as a precursor (Fig. 16). Using this method, the advantages may be retained, the preparation of these precursors should be relatively easy and better yields should observed. For instance, preliminary results of the pyrolysis of a cyclic phosphazene trimer containing $CpRu(PPh_3)_2^+$ affords mainly nanostructured RuO_2. Further experiments of pyrolysis with other organometallic fragments are in under way.

ACKNOWLEDGMENTS

We acknowledge with thanks the financial support under FONDECYT Project 1030515.

REFERENCES

1. (a) D. O'Hare and D. W. Bruce. *Inorganic Materials* (John Wiley & Sons, Chichester UK, 1992). (b) N. J. Coville and L. Cheng, *J. Organomet. Chem.* **571**, 149 (1998). (c) P. J. Pickup. *J. Mater. Chem.* **9**, 1641 (1999). (d) F. Ciardelli, E. Tsuchida, and D. Wohrle, *Macromolecule–Metal Complexes* (Springer, Berlin, 1996). (e) C. U. Pittman Jr, C. E. Carraher, M. Zeldin, J. E. Sheats, and B. M. Culbertson, *Metal-containing Polymeric Material* (Plenum, New York, 1996). (f) P. Wisian-Neilson, H. R. Allcock and K. J. Wynne, *Inorganic and Organometallic Polymers II; Advanced Material and Intermediates* (ACS Sym. Ser. 572, 1994).
2. (a) P. Nguyen, P. Gomez-Elipe, and I. Manners, *Chem. Rev.* **99**, 1515 (1999). (b) I. Manners, *J. Chem. Commun.* 857 (1999). (c) R. P. Kingsborough and T. M. Swager, *Progr. Inorg. Chem.* **48**, 123 (1999).
3. (a) H. R. Allcock, *Adv. Mater.* **6**, 106 (1994). (b) I. Manners, *Angew. Chem. Int. Ed. Engl.* **35**, 1602 (1996).

4. (a) M. Gleria, R. De Jaeger (Eds), *Phosphazenes: A World Wide Insight* (Nova Science Publishers, New York, 2004). (b) H. R. Allcock, *Chemistry and Applications of Polyphosphazenes* (John Wiley & Sons, Hobokan, New York, 2003).
5. (a) A. S. Edelstein and R. C. Cammarata, *Nanomaterials: Synthesis Properties and Applications*, (J. W. Arrowsmith Ltd., eds. Bristol, 2000). (b) K. J. Klabunde, *Nanoscale Materials in Chemistry* (Wiley-Interscience, New York, 2001).
6. (a) J. Grunes, J. Gabor, and A. Somorjai, *Chem. Commun.* 2257 (2003). (b) A. T. Bell, *Science* **299**, 1688 (2003).
7. M. Ginzburg, M. J. MacLachlan, S. MingYang, N. Coombs, T. W. Coyle, N. Praju, J. E. Greendan, R. H. Herber, G. A. Ozin, and I. Manners, *J. Am. Chem. Soc.* **124**, 2625 (2002).
8. R. Petersen, D. A. Foucher, B. Tang, A. Lough, N. Praju, J. E. Greedan, R. H. Herber, and I. Manners, *Chem. Mater.* **7**, 2045 (1995).
9. T. Terenish, S. Hasegawa, T. Shimizu, and M. Miyake, *Adv. Mater.* **13**, 1699 (2001).
10. T. Shimizu, T. Teranishi, S. Hasegawa, and M. Miyake, *J. Phys. Chem.* **107**, 2719 (2003).
11. J. Qiu, X. Jiang, C. Zhu, M. Shirai, and N. J. Jiang, *Angew Chem. Int. Ed.* **43**, 2230 (2004).
12. E. R. Leite, N. L. V. Carreño, E. Lango, Pontes F. M., A. Barison, A. G. Ferreiro, Y. Maniette, and J. A. Varela, *Chem. Mater.* **14**, 3722 (2002).
13. D. L. Boxall, E. A. Kenik, and C. M. Lukehart, *Chem. Mater.* **14**, 1715 (2002).
14. A. Roucoux, J. Schulz, and H. Patin, *Chem. Rev.* **102**, 3757 (2002).
15. C. Díaz and M. L. Valenzuela, in *Horizons in Polymer Research*, R. B. Bregg, ed. (Nova Science Publishers, 2005), Chapter 6.
16. C. Díaz and P. Castillo, *J. Inorg. Organomet. Polym.* **11**, 183 (2002).
17. G. A. Carriedo, F. J. García Alonso, P. Gonzalez, and P. Gomez-Elipe, *Polyhedron* **18**, 2853 (1999).
18. C. Díaz, P. Castillo, G. A. Carriedo, P. Gómez-Elipe, and F. J. García Alonso, *Macromol. Phys. Chem.* **203**, 1912 (2002).
19. G. A. Carriedo, F. J. García Alonso, P. Gómez-Elipe, C. Díaz, and N. Yutronic, *J. Chilean Chem. Soc.* **48**, 25 (2003).
20. C. Díaz and P. Castillo, *Polym Bull.* **50**, 123 (2003).
21. C. Díaz, M. L. Valenzuela, and M. Barbosa, *Mater. Res. Bull.* **39**, 9 (2004).
22. G. A. Carriedo, F. J. García Alonso, J. L. García Álvarez, C. Díaz, and N. Yutronic, *Polyhedron* **21**, 2587 (2000).
23. M. A. Olshavsky and H. R. Allcock, *Chem. Mater.* **9**, 1367 (1997).
24. C. H. Walker, J. V. St. John, and P. Wisian-Neilson, *J. Am. Chem. Soc.* **123**, 3846 (2001).
25. J. Jung, T. Kmecko, C. L. Claypool, H. Zhang, and P. Wisian-Neilson, *Macromolecules* **38**, 2122 (2005).
26. G. A. Carriedo, F. J. García Alonso, C. Díaz, and M. L. Valenzuela, *Polyhedron* **25**, 105 (2006).
27. C. Díaz, P. Castillo, and M. L. Valenzuela, *J. Cluster Sci.* **16**, 515 (2006).
28. C. Diaz and M. L. Valenzuela, *Macromolecules* **39**, 103 (2005).
29. G. A. Carriedo, F. J. García Alonso, J. L. García Álvarez, C. Díaz, and N. Yutronic, *Polyhedron* **21**, 2579 (2000).
30. C. Diaz and M. L. Valenzuela, *J. Inorg. Organomet. Polym.* **16**, 123 (2006).
31. C. Díaz, M. L. Valenzuela, E. Spodine, Y. Moreno, and O. Peña, submitted.
32. M. Valle, J. López-Ruiz, J. M. Badia, and P. Adeva, *Microscopia Electrónica de Barrido y Microanálisis por Rayos X*, Chapter 23. (Rueda, Madrid, 1996).
33. F. A. Cotton and J. T. Mague, *Inorg. Chem.* **5**, 317 (1966).
34. C. Díaz, F. J. García-Alonso, G. Carriedo, and M. L. Valenzuela, Unpublished results.
35. C. Díaz, M. L. Valenzuela, and N.Yutronic. J. Inorg. Organomet. Polym. Mater. (2006). In press.
36. K. Akamatsu, T. Kawamura, H. Nabira, S. Deki, T. Strunskus, and F. Faupel, *J. Mater. Chem.* **12**, 3610 (2002).
37. S. Nath, S. Praharay, S. Panigrahi, S. Kumar Ghosh, S. Kundu, S. Basu, and T. Pol, *Langmuir* **21**, 10405 (2005).
38. H. Yu, M. Chen, P. M. Rice, S. X. Wang, R. L. Whiteand, and S. Sun, *Nano. Lett.* **5**, 379 (2005).
39. C. Diaz, M. L. Valenzuela, A. Laguna, I. Jimenez, Unpublished results.
40. C. Diaz, M. L. Valenzuela, D. Abizanda, I. Jimenez, and A. Laguna. J. Inorg. Organomet. Polym. Mater. (2006) In Press.
41. F. Dachille and L. Dent-Glasser, *Acta Crytallogr.* **12**, 280 (1959).
42. H. R. Allcock and D. J. Brennan, *J. Organomet. Chem.* **341**, 231 (1998).
43. H. R. Allcock, D. J. Brennan, and B. S. Dunn, *Macromolecules* **22**, 1534 (1989).
44. H. R. Allcock, W. D. Coggio, R. S. Archibald, and D. J. Brennan, *Macromolecules* **22**, 3571 (1989).
45. H. R. Allcock and W. D. Coggio, *Macromolecules* **23**, 1629 (1990).
46. H. R. Allcock, S. E. Kuhercik, and C. J. Nelson, *Macromolecules* **29**, 3686 (1996).
47. H. R. Allcock and S. E. Kuhercik, *J. Inorg. Organomet. Polym.* **5**, 307 (1995).
48. H. R. Allcock and S. E. Kuhercik, *J. Inorg. Organomet. Polym.* **6**, 1 (1996).
49. G. A. Carriedo, F. J. García Alonso, A. Presa, C. Diaz, M. L.Valenzuela, Unpublished results.